Cell Reports
Medicine

Report

Type I interferon exposure of an implantation-on-a-chip device alters invasive extravillous trophoblast function

Graphical abstract

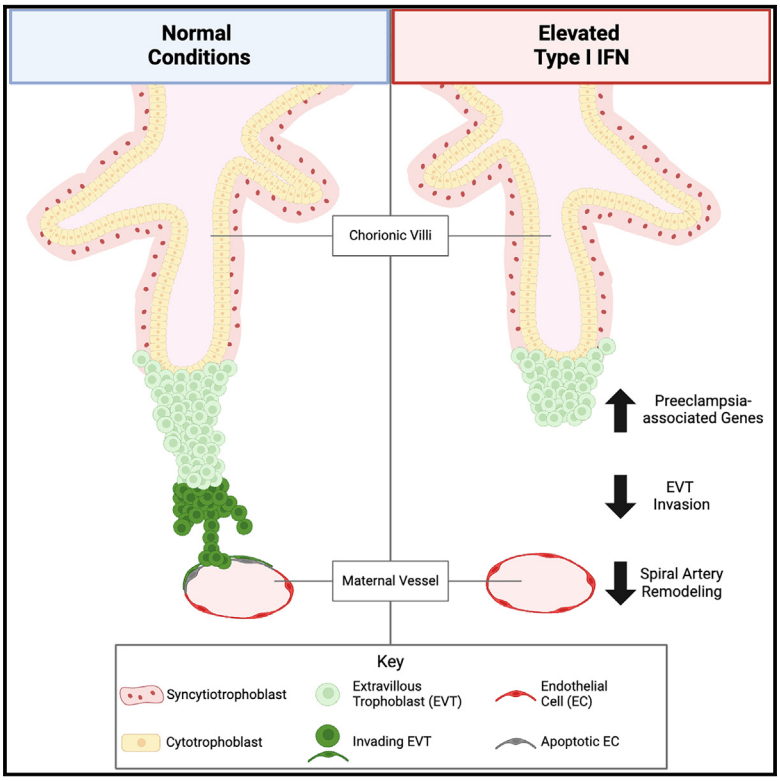

Highlights

- Elevated type I interferon (IFN) abrogates extravillous trophoblast (EVT) invasion
- EVT exposure to IFNb limits the emergence of invading EVTs
- IFN stimulation promotes preeclamptic gene signature in EVTs
- EVT-directed vascular remodeling is limited by type I IFN

Authors

Michael K. Simoni, Seble G. Negatu, Ju Young Park, ..., Dan Dongeun Huh, Monica Mainigi, Kellie A. Jurado

Correspondence

monica.mainigi@pennmedicine.upenn.edu (M.M.), kellie.jurado@pennmedicine.upenn.edu (K.A.J.)

In brief

Simoni, Negatu et al. use an implantation-on-a-chip device to evaluate the consequence of elevated type I IFN exposure on implantation. Using single-cell transcriptomes, they uncover that type I IFN exposure alters extravillous trophoblast invasion and induces preeclampsia-associated genes, implicating unwarranted type I IFN as a maternal disturbance that can trigger preeclampsia.

Simoni et al., 2025, Cell Reports Medicine 6, 101991
March 18, 2025
https://doi.org/10.1016/j.xcrm.2025.101991

CellPress

Cell Reports Medicine

CellPress
OPEN ACCESS

Report

Type I interferon exposure of an implantation-on-a-chip device alters invasive extravillous trophoblast function

Michael K. Simoni,[2,4] Seble G. Negatu,[1,4] Ju Young Park,[3] Sneha Mani,[2] Montserrat C. Arreguin,[1] Kevin R. Amses,[1] Dan Dongeun Huh,[3] Monica Mainigi,[2,*] and Kellie A. Jurado[1,5,*]

[1]Department of Microbiology, University of Pennsylvania Perelman School of Medicine, Philadelphia, PA 19104, USA
[2]Department of Obstetrics and Gynecology, Hospital at the University of Pennsylvania, Philadelphia, PA 19104, USA
[3]Department of Bioengineering, University of Pennsylvania, Philadelphia, PA 19104, USA
[4]These authors contributed equally
[5]Lead contact
*Correspondence: monica.mainigi@pennmedicine.upenn.edu (M.M.), kellie.jurado@pennmedicine.upenn.edu (K.A.J.)
https://doi.org/10.1016/j.xcrm.2025.101991

SUMMARY

Inappropriate type I interferon (IFN) signaling during embryo implantation and placentation is linked to poor pregnancy outcomes. Here, we evaluate the consequence of elevated type I IFN exposure on implantation using a human implantation in an organ-on-a-chip device. We reveal that type I IFN reduces extravillous trophoblast (EVT) invasion capacity. Analyzing single-cell transcriptomes, we uncover that IFN truncates invasive EVT emergence in the implantation-on-a-chip device by stunting EVT epithelial-to-mesenchymal transition. Disruptions to the epithelial-to-mesenchymal transition are associated with the pathogenesis of preeclampsia, a life-threatening disorder of pregnancy. Strikingly, IFN stimulation induces genes associated with increased preeclampsia risk in EVTs. These dysregulated EVT phenotypes ultimately reduce EVT-mediated endothelial cell vascular remodeling in the implantation-on-a-chip device. Overall, our work implicates unwarranted type I IFN as a maternal disturbance that can result in abnormal EVT function that could trigger preeclampsia.

INTRODUCTION

Balanced immune-mediated intercellular communication underlies successful reproduction.[1] Embryo implantation into the maternal endometrium, and subsequent placentation, is a complex process where fetal trophoblast cells invade and restructure the uterine vasculature. Endometrial transformation enables low resistance blood flow to the fetus and requires a precise degree of trophoblast invasion in order to prevent placental dysfunction. Either inadequate or excessive trophoblast invasion can lead to a wide spectrum of pregnancy complications, and thereby requires fine-tuned control. Extravillous trophoblasts (EVTs) arise from epithelial cytotrophoblasts (CTBs) with specialized migratory and invasive properties and mediate endometrial invasion and spiral artery remodeling. EVT functionality is tightly regulated by many different cell types including uterine immune cells via cytokine mediator.[1,2] Growing literature indicates interferons (IFNs) as cytokine mediators required for proper endometrial decidualization and spinal artery remodeling under normal physiological conditions,[3–5] albeit the producers remain unknown.

Maternal immune dysregulation and inflammation are linked to various pregnancy complications. Chronic inflammatory conditions, such as systemic lupus erythematosus (SLE), are associated with an elevated risk of pregnancy loss.[6–8] Specifically, patients with lupus flares during early pregnancy are at a greatest risk for pregnancy complications, with a 30%–40% chance of suffering a pregnancy loss.[6] Studies have specifically linked inappropriate type I IFN signaling during early pregnancy, when embryo implantation and placentation occur, with poor pregnancy outcomes. For example, patients with SLE that developed preeclampsia (PE) were found to have higher functional type I IFN activity early in pregnancy compared to patients with SLE who had uncomplicated pregnancies.[9] Type I IFN signaling typically drives an antiviral state but can also be elevated in certain states of immune dysregulation and/or autoimmune conditions, including SLE.[8] PE complicates 13%–35% of SLE pregnancies, compared to less than 1%–6% in otherwise healthy women.[10] PE is a hypertensive disorder in pregnancy that is characterized by shallow trophoblast invasion and inadequate spiral artery remodeling. Given that type I IFN is elevated in patients with SLE who demonstrated pregnancy complications associated with poor trophoblast invasion, we hypothesized that elevated type I IFN during early pregnancy could impact EVT function and lead to a stressed villous placenta, thereby increasing the risk of developing PE.

This led us to investigate the impact of elevated type I IFN stimulation on EVT invasion and spiral artery remodeling. Using a biomimetic model of human implantation in a microengineered

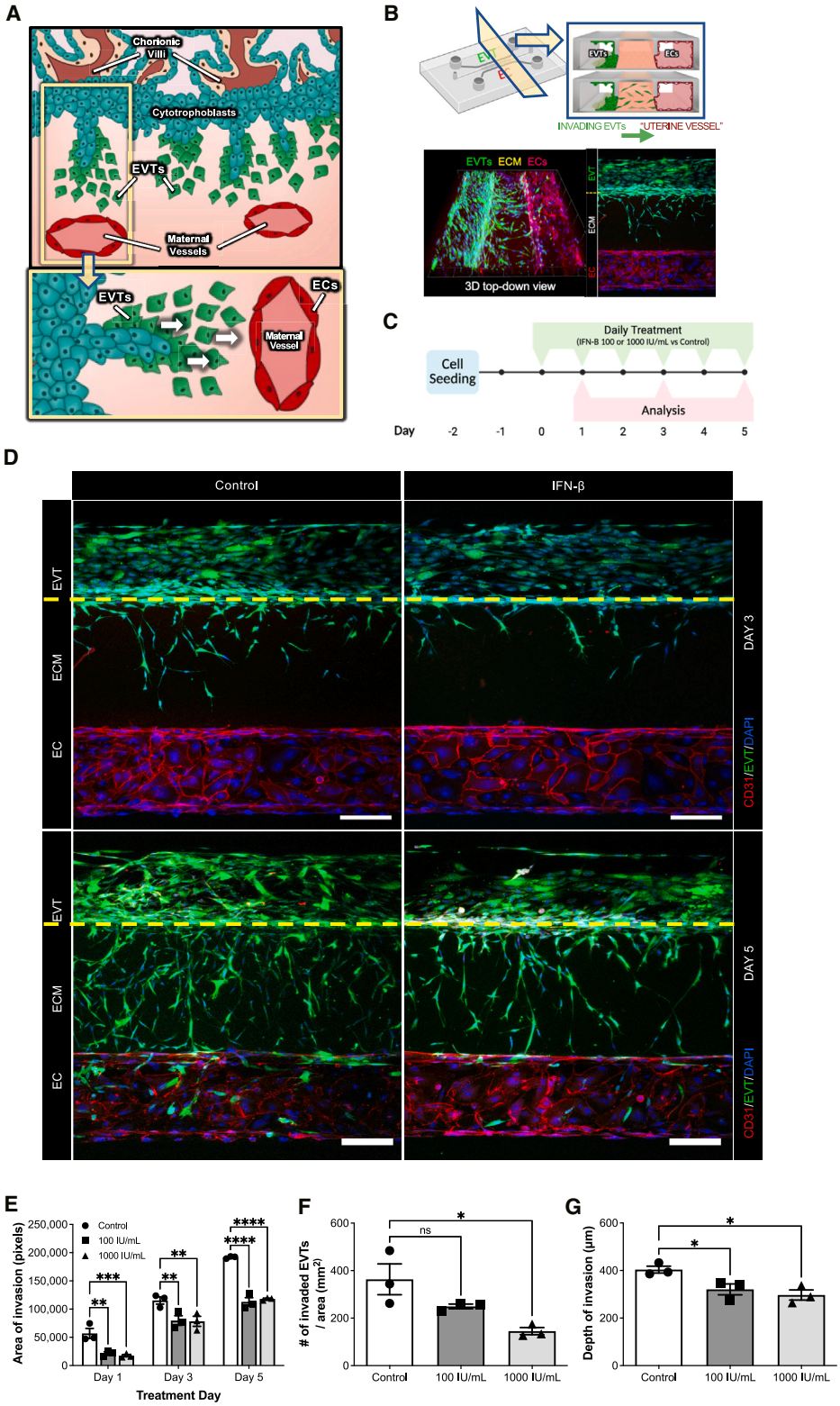

Figure 1. Type I interferon exposure abrogates EVT invasion

(A) A visual portrayal of human embryo implantation, where cytotrophoblasts, present within the fetal chorionic villi, differentiate into extravillous trophoblasts (EVTs) that invade into the maternal uterus toward maternal vasculature.

(legend continued on next page)

organ-on-a-chip device,[11] we found that exposure to type I IFN abrogated EVT invasion. Analyzing single-cell transcriptomic data obtained from cells extracted from devices, we found that unwarranted type I IFN exposure limits endovascular EVT emergence, disrupts EVT epithelial-to-mesenchymal (EMT) progression, and induces a preeclamptic gene signature in EVTs. These dysregulated phenotypes ultimately reduced EVT-mediated vascular remodeling in our implantation-on-a-chip (IOC) device. Our findings implicate unwarranted type I IFN as a maternal disturbance that can trigger PE.

RESULTS

Elevated type I IFN exposure abrogates EVT invasion

Since higher functional type I IFN activity early in pregnancy was detected in patients with SLE who developed PE compared to patients with SLE with uncomplicated pregnancies,[9] we aimed to assess the impact of elevated type I IFN on implantation. To do this, we employed an IOC device that models the invasion of fetal EVTs into the maternal uterus.[11] The IOC device reconstructs the three-dimensional organization of the maternal-fetal interface where EVTs exhibit directional migration through an extracellular matrix (ECM) toward endometrial endothelial cells (ECs) (Figures 1A and 1B). EVT migration within the IOC device is dependent on intercellular communication with maternal endometrial ECs, highlighting its physiological relevance.[11] To begin, we seeded the IOC device with primary human first trimester histocompatibility leukocyte antigen (HLA)-G+ EVTs isolated from clinical specimens and primary human endometrial ECs. EVT expression of human placental lactogen (HPL), cytokeratin-7 (Ck7), and HLA-G was confirmed using immunofluorescent staining (Figure S1A). Two days after seeding, we began daily treatments of EVTs and ECs in the IOC device with IFN-β (100 or 1,000 IU/mL, as previously used/established[12]), a hallmark type I IFN, by supplementing the daily media exchange. Media disperses throughout the chip upon addition, thereby exposing both cell types to IFN-β. We next assessed the properties of EVT invasion into the ECM toward the endothelial chamber for 5 days (Figure 1C). Within 24 h of IFN-β treatment, we observed a significant reduction in EVT migration out of the trophoblast chamber and into the ECM as compared with the control (Figures 1D and 1E). This blunting of EVT invasion with IFN-β exposure persisted at day 3 and 5 (Figures 1D and 1E). At day 5 post IFN-β exposure, we quantified the depth of invasion and the number of EVTs invaded into the ECM. Using these measurements, we observed that both the average number of invaded EVTs and the average depth of EVTs in the ECM were significantly reduced after 1,000 IFN-β IU/mL exposure (Figures 1F and 1G). Using a lower dose of IFN-β (100 IU/mL), we observed similar abrogation of EVT invasion with significant reductions in the average depth of EVTs in the ECM and a trend in reduced EVT invasion (Figures 1E–1G).

Next, we evaluated if IFN-β exposure impacted cellular proliferation. Previously, we found that primary EVTs, marked by the co-expression of Ki-67 and HLA-G, proliferate on the IOC device in the presence of endometrial ECs.[8] Furthermore, recent literature using spatial transcriptomics of patient implantation site samples revealed that EVTs proliferate *in vivo*.[13] We first validated this proliferation using immunofluorescent staining of EVTs in our model that showed co-expression of Ki-67 and HLA-G (Figure S1A). Following this, upon staining for Ki-67 on the IOC device, we noted a decrease in Ki-67 expression at 3 and 5 days post IFN-β exposure as compared with control (Figure S1B), indicating a reduction in EVT proliferative capacity after prolonged IFN-β exposure. Taken together, these findings indicate that elevated type I IFN exposure impairs EVT invasive capacity.

Elevated type I IFN limits invading EVT emergence

To investigate how elevated IFN-β exposure impacts EVT invasion, we next determined the transcriptomes of cells isolated from the IOC device via single-cell sequencing (scRNA-seq). At 5 days post IFN-β exposure or PBS control, we extracted 38,495 cells from all layers of 36 IOC devices and processed for 10× Genomics. Raw counts were filtered for empty cells, doublets, and other quality control parameters. We used Seurat (v.4.0.4) to combine all samples into a single object, and as expected, uniform manifold approximation and projection (UMAP) dimensionality reduction yielded two primary groups of cells (Figure 2A). Cellular markers unique to EVTs and ECs were used to distinguish the identity of each primary cell group. Expression of trophoblast glycoprotein (*TPBG*) and placenta-specific protein 9 (*PLAC9*) broadly distinguished trophoblast clusters from ECs, while EC clusters were determined by CD31 (*PECAM1*) and von Willebrand factor (VWF) expression (Figure 2B). Despite HLA-G protein expression within EVTs (Figure S1A), EVT clusters had low levels of HLA-G transcripts (Figure S1C). Further, relative to ECs, EVTs had diminished HLA-A expression (Figure S1D). Clustertree analysis with a resolution of 0.2 resulted in four clusters within the EVT group, and two within the EC group, indicating cell state heterogeneity among EVTs and ECs.

Upon trophoblast invasion into the maternal endometrium, EVTs remodel and replace the maternal endothelium of uterine arteries in order to promote low resistance blood flow to the

(B) Top left: schematic of the implantation-on-a-chip (IOC) microfluidics device. The center and two side lanes have dimensions of 0.5 mm (width) × 0.3 mm (height) and 0.25 mm (width) × 0.3 mm (height), respectively. Top right: compartmentalized design of the IOC device allows EVTs to migrate through an extracellular matrix (ECM) toward maternal endothelial cells (ECs). Bottom row: 3D (left) and 2D top-down (right) representative images of EVTs (green: CellTracker Green) migrating across the ECM hydrogel toward maternal ECs (red: CD31).
(C) Graphic of experimental timeline shown in days with start of type I interferon (IFN-β) treatment at day 0.
(D) Representative image of IOC device at day 3 (top row) and day 5 (bottom row) with EVTs (green: CellTracker Green) migrating toward maternal ECs (red: CD31) in control and after IFN-β (1,000 IU/mL) exposure; scale bars, 200 μm. Representative images are from three independent experiments.
(E) Quantification of EVT area invasion at day 1, 3, and 5.
(F and G) Quantification of number of invaded EVTs (F) and depth of invasion (G) at day 5 post treatment.
Data are presented as mean ± SEM (n = 3 independent devices per group). two-way ANOVA with Tukey's multiple comparison test (E). One-way ANOVA with Dunnett's multiple comparison test (F and G). ns, $p > 0.05$; *$p < 0.05$; **$p < 0.01$; ***$p < 0.001$; ****$p < 0.0001$ (n = 3 independent devices per group).

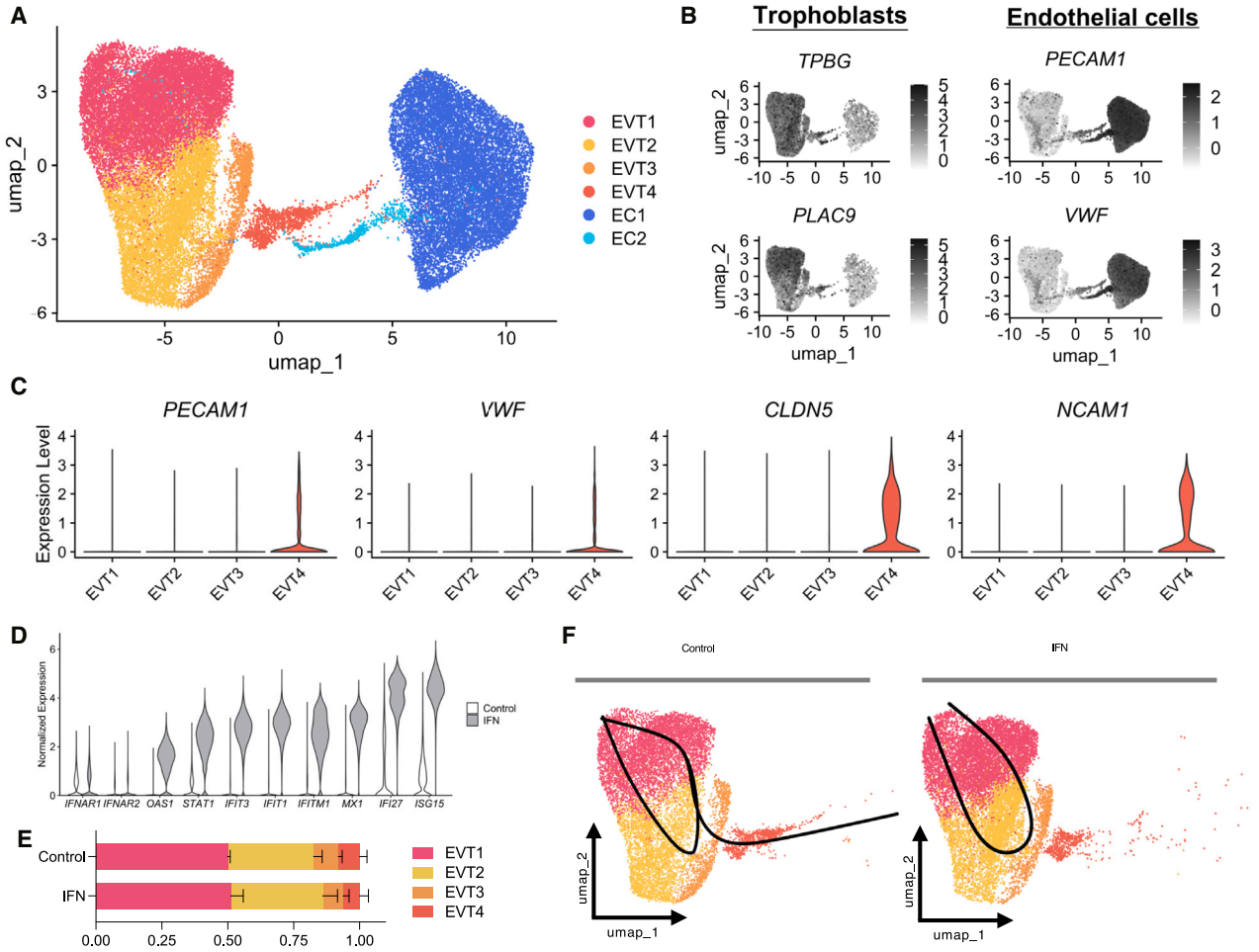

Figure 2. Elevated type I interferon limits invading extravillous trophoblast emergence

(A) Uniform manifold approximation and projection (UMAP) plot of scRNA-seq of cells within 36 implantation-on-chip (IOC) devices (n = 38,495 cells) colored by cell type and state.

(B) UMAP plot of marker genes characteristic of trophoblasts (left) and endothelial cells (right).

(C) Violin plots showing normalized and log-transformed expression of genes characteristic of endovascular EVTs in individual EVT subsets (x axis).

(D) Violin plots showing normalized expression of the type I IFN receptor subunits (*IFNAR1* and *IFNAR2*) and representative interferon (IFN)-stimulated genes (x axis) from scRNA-seq data in all cells in the IOC device separated by control (white) and type I IFN-exposed cells (gray).

(E) Bar plot representing the proportion of EVT subsets separated by control and IFN-stimulated cells. Data are presented as mean ± SEM.

(F) Minimum spanning tree computed by Slingshot, visualized on the UMAP of EVT subsets, separated by control and type I IFN-stimulated cells.

placenta. EVTs will adopt an endothelial-like state during endovascular invasion.[14,15] Fascinatingly, the UMAP yielded a convergence of transcriptomes between the two primary cell types (Figure 2A). Furthermore, the cellular cluster at convergence, EVT4, uniquely expressed endothelial markers *PECAM1*, *VWF*, and *CLDN5* along with the well-described marker of endovascular trophoblasts, *NCAM1* (Figure 2C).[14,16] To further benchmark EVT4s, we integrated single-nucleus RNA sequencing data from ~2,000 interstitial and endovascular EVTs from a reference human implantation site[13] and identified a substantial overlap with EVT4s (cluster 3 in Figures 2B and 2C). Incredibly, these data support that invading EVTs emerge within the IOC device.

When IFN-β binds to the type I IFN receptor complex (IFN-α receptor [IFNAR]), it initiates signaling through the Janus kinase-signal transducer and activator of transcription pathway and leads to the transcription of many IFN-stimulated genes (ISGs). We first confirmed the expression of the *IFNAR1* and *IFNAR2* subunits (Figure 2D). Next, upon evaluation of ISG induction following IFN-β treatment, we observed the expression of several canonical ISGs (*IFI27*, *IFIT1*, *IFIT3*, *IFITM1*, *ISG15*, *MX1*, *OAS1*, and *STAT1*) across all EVT and EC clusters that were exposed to IFN-β as compared to control (Figure 2D), indicating a robust response to cytokine stimulation. We next quantified the proportion of cells within clusters to assess the impact of type I IFN exposure on cell type heterogeneity. Consistent with invasion assays (Figure 1), the changes were primarily observed among the EVT clusters that represent the convergence between the two cell types: EVT3 and EVT4 (Figure 2A). EVT3 and EVT4 clusters' proportions decreased after IFN-β exposure, albeit not statistically significant (Figure 2E). We next used Slingshot to resolve subset emergence

in pseudotime within both control EVTs and in IFN-β-exposed EVTs (Figure 2F).[17] Intriguingly, trajectory analysis predicted a loss of trajectory toward EVT4 in the type I IFN-treated EVTs compared to control EVTs (Figure 2F). This truncation in emergence progression was also supported by an alternative trajectory analysis platform, Monocle3 (Figure S3A).[18] Concurrently, we evaluated changes in EVT cell state using an RNA velocity package, velocytoR, that evaluates spliced/unspliced matrices.[19] Truncated RNA velocity vectors in EVT3 and EVT4 supported limited changes in cell state with IFN treatment compared to control (Figure S3B). Collectively, from these data, we conclude that elevated type I IFN exposure limited the emergence of invading EVTs in the IOC device.

Elevated type I IFN alters EMT transition and promotes a preeclamptic gene signature in EVTs

EMT is a dynamic transformation of cellular organization from an epithelial state to a mesenchymal phenotype and leads to the functional acquisition of cellular migration and invasion. CTB to EVT differentiation is a unique form of EMT where EVTs exist along a spectrum of mixed epithelial and mesenchymal states that can readily interconvert (Figure 3A).[20,21] Gene expression analyses of primary CTBs and EVTs have revealed dynamic gene signatures along the EMT spectrum.[20–23] Specifically, first trimester EVTs display more developed mesenchymal features during active endometrial remodeling as compared with third trimester EVTs, which comparatively present with more epithelial features.[20] This epithelial-to-mesenchymal plasticity ensures that EVT migration and invasion can be regulated by decidual checkpoints to avoid pathogenic outcomes.[23]

Given that EVTs for the IOC device were isolated from first-trimester placental villi, we sought to evaluate changes in mesenchymal and epithelial genes previously described in primary EVTs.[21] All EVTs expressed high levels of mesenchymal genes (*FN1*, *VIM*, and *RHOC*) and transcription factors (*SNAI2* and *TCF-4*) in addition to lower levels of epithelial genes (*KRT18*, *CTNNB1*, and *SERPINE1*) and transcription factors (*TWIST* and *FOXC2*) (Figure 3B). We noted that EVT1s expressed higher levels of genes characteristic of a more developed mesenchymal phenotype, including genes involved in invasion (*MMP2*) and motility (*SPARC*), ECM deposition (*DCN*, *LUM*, and *COL1A1*) (Figure 3C). In contrast, EVT2s more distinctly expressed regulatory inducers of EMT (*HMGA1*, *HMGA2*, *PHLDA2*, and *STC1*).[24–27] Interestingly, the trajectory analysis on EVTs in Figure 2F proposes a pathway of interconversion between EVT1 and EVT2 clusters and thereby might represent the plasticity of EVTs along the epithelial-to-mesenchymal spectrum (Figure 3A).

Notably, exposure to type I IFN resulted in several classical mesenchymal genes to be considerably reduced in all EVTs (Figure 3D). This included decreased expression of canonical mesenchymal markers such as *VIM* and *RHOC* and ECM proteins (*COL1A1*). Furthermore, we saw reduced expression of genes involved in cell motility (TAGLN, ACTA2, and *ACTG1*) and mesenchymal integrins (*ITGAE* and *ITGAV*). From this, we deduce that unwarranted type I IFN leads to a stunted epithelial-to-mesenchymal progression in EVTs.

Disruptions to EMT are associated with the pathogenesis of PE.[28,29] PE is characterized by shallow trophoblast invasion and a failure to adequately remodel spiral arteries; therefore, we next evaluated genes known to be associated with PE pathophysiology (Figure 3E). We found heightened expression of several genes associated with increased PE risk including *TNFSF13B*, *TFPI2*, *TIMP3*, *RBM25*, *IGF2R*, and *CSF1*[28,30–32] in IFN-EVTs compared with control EVTs (Figure 3E). We also observed increased expression of complement activation components that have specifically been implicated in PE pathogenesis (*CFH*, *CFB*, *C1R*, and *C1S*) in IFN-exposed EVTs.[33,34] Given these associations, we next compared our list of differentially expressed genes in IFN-exposed EVTs with a list of dysregulated genes in EVTs from single-cell transcriptomes of EVTs in patients with PE recently published by Admati et al.[35] We identified noteworthy overlap with 20% of upregulated genes and 26% of downregulated genes shared with dysregulated EVT genes found in patients with PE (Figure 3F). Taken together, these data indicate that elevated type I IFN exposure disrupts EVT-EMT progression and results in a PE-like gene signature in EVTs.

Elevated type I IFN limits EVT-mediated vascular remodeling in the IOC device

Spiral artery remodeling is critical for enabling adequate blood supply to the fetus and involves the replacement of luminal ECs in uterine arteries with endovascular trophoblast. Physiological transformation of maternal vasculature is a dynamic process that is mediated by EVTs. Vascular disruption and endothelial apoptosis are two major features of spiral artery remodeling upon endovascular EVT invasion. Notably, the IOC device models these processes in a physiologically relevant manner.[11] Since we observed that type I IFN exposure impaired EVT invasion in the IOC and reduced invading EVT emergence and overall EVT quality, we next aimed to ask if this ultimately impacted EVT-induced vascular remodeling. To begin, we resolved the most likely trajectory of cell state emergence in pseudotime among all ECs via Slingshot. We found that the primary cluster of EC1 transitions into the minor EC2 cluster, indicating that EC2s are undergoing a transformation of cell state (Figure 4A). In order to ask if EC2s are representative of ECs undergoing remodeling, we next assessed the expression of an important adhesion protein commonly used to distinguish vascular disruption during implantation, vascular endothelial cadherin (*CDH5*). We found that EC2 had decreased *CDH5* levels as compared with EC1 (Figure 4B), data suggestive that EC2 might represent cells within the endothelial population that are actively undergoing remodeling.

To explore further, we next evaluated differentially expressed genes in EC2s as compared with EC1s. Among the most upregulated genes in EC2s were various apoptosis regulatory long-coding RNAs such as *MALAT1*, *MTRNR2L12*, and *NEAT1* (Figure 4C). Consistently EC2s had decreased expression of anti-apoptotic genes, where we saw lower levels of the caspase inhibitor CARD16 (*CARD16*) and the anti-apoptotic (*COX5A*).[36,37] In further support of EC2s transitioning to increased apoptotic state, we observed enhanced expression of mitochondrial cytochrome *c* subunits (*MT-CO1*, *MT-CO2*, and *MT-CO3*)[38] and reduced expression of various ribosomal proteins (*RPS8*, *RPL13*, and *RPL18*).[39] Lastly, we noted that EC2s had lower levels of genes associated with contraction (*VAMP5*, *MYL12A*, and *MYL12B*) as

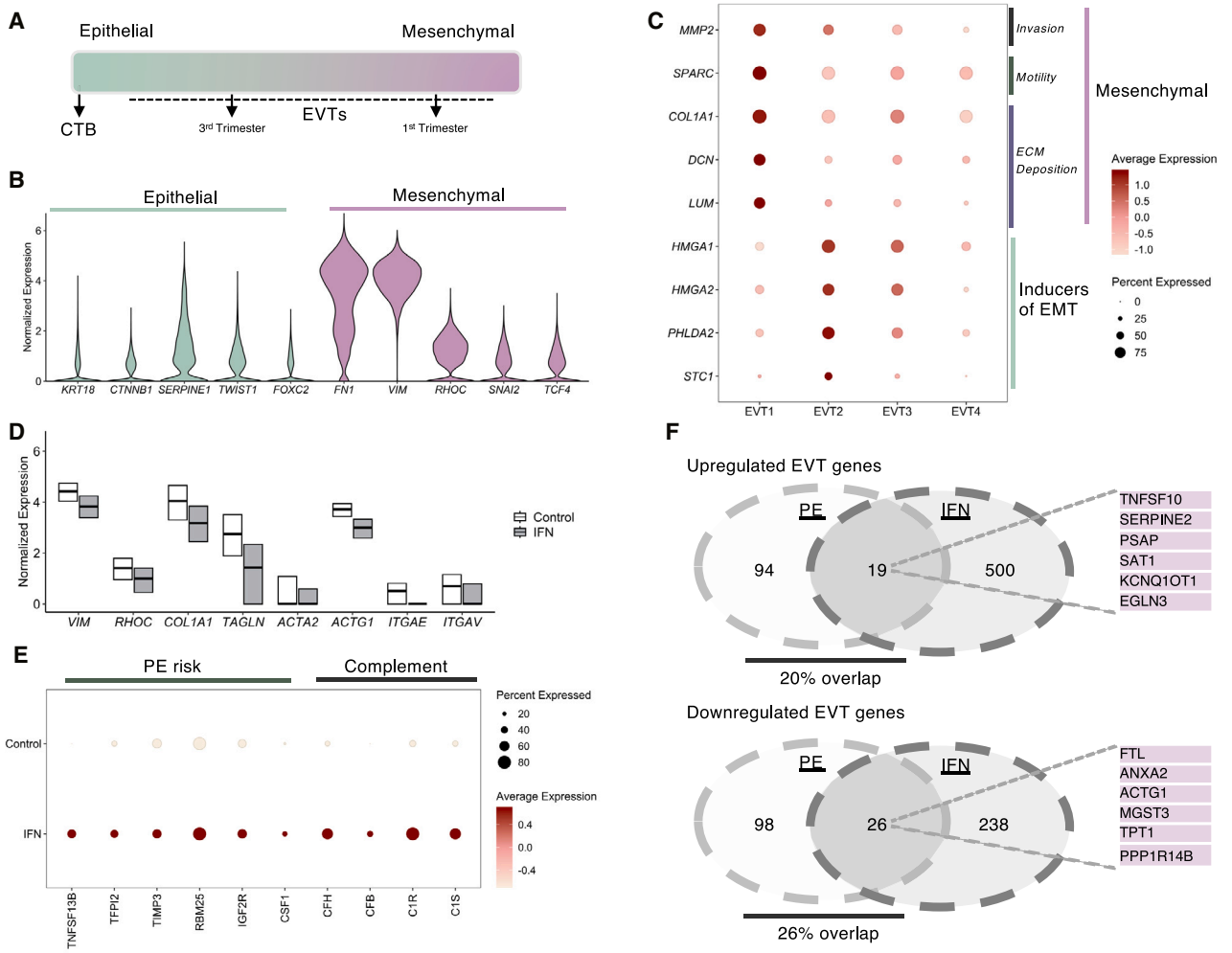

Figure 3. Elevated type I interferon alters epithelial-to-mesenchymal transition and promotes a preeclamptic gene signature in extravillous trophoblasts

(A) Schematic describing the dynamic spectrum of epithelial-to-mesenchymal transition (EMT) in cytotrophoblast to extravillous trophoblast (EVTs) transition. Small arrows indicate that first trimester EVTs display more developed mesenchymal features during active endometrial remodeling as compared with third trimester EVTs.

(B) Violin plots showing normalized expression of representative canonical epithelial genes (left) and mesenchymal genes (right) in all EVT cells.

(C) Dot plots showing normalized, log-transformed, and variance-scaled expression of genes characteristic of mesenchymal genes and regulatory, inducers of EMT (y axis) in individual EVT subsets (x axis).

(D) Boxplot showing normalized, classical mesenchymal genes in all EVT cells separated by control (white) and IFN-stimulated cells (gray).

(E) Dot plots showing normalized, log-transformed, and variance-scaled expression of preeclampsia risk factors (x axis) in all EVT separated by control and IFN-stimulated cells (y axis).

(F) Venn diagram of dysregulated genes in EVTs from patients with PE with early- and late-onset preeclampsia with our list of differentially expressed genes in IFN-exposed EVTs (upregulated and downregulated genes had a false detection rate less 5% and log fold change greater than one). Representative genes that overlap are listed to the right.

compared with EC1s, indicating differences in EC functionality. Collectively, the gene expression signature of EC2s supports that this population is undergoing apoptotic remodeling.

We next assessed if IFN-β exposure ultimately impacted EVT-mediated apoptosis by evaluating the percent mitochondrial RNA in EC clusters within our sequencing data, a proxy for apoptotic cell fate.[40] We observed an increased percentage of mitochondrial genes in both control EC clusters as compared to IFN-exposed EC clusters (Figure 4D), suggestive of less apoptotic remodeling in IFN-exposed ECs. Upon comparing differentially expressed genes between control EC clusters with IFN-exposed clusters, as expected, we primarily observed increased changes in IFN signaling genes (Table S1). Next, we aimed to corroborate this finding of distinct cell death between conditions by staining the IOC device for activated, cleaved caspase-3 (Figure 4E). Consistently, we found that IFN-β treatment limited EVT-mediated apoptosis within the IOC device, which significantly reduced the amount of cleaved caspase-3

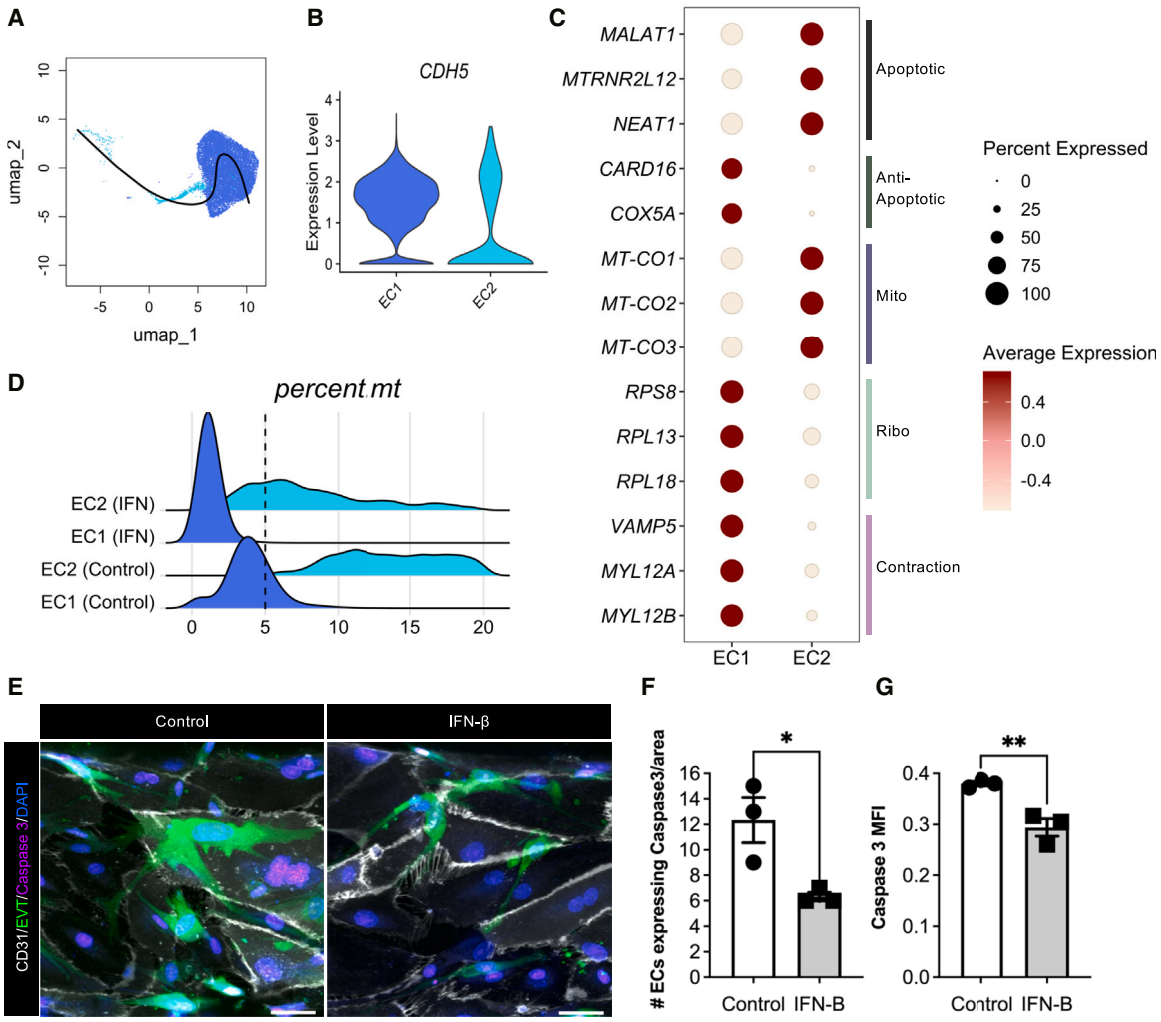

Figure 4. EVT-directed vascular remodeling is limited by type I interferon

(A) Minimum spanning tree computed by Slingshot, visualized on the UMAP of EC subsets, EC1 (dark blue) and EC2 (light blue).

(B) Violin plots showing normalized expression of VE-cadherin (CDH5) in individual EC subsets (x axis).

(C) Dot plots showing normalized, log-transformed, and variance-scaled expression of genes characteristic of progression toward an apoptotic state and endothelial function (y axis) in individual EC subsets (x axis).

(D) Percent mitochondrial gene expression (x axis) in individual EC subsets, separated by control (bottom) and IFN-stimulated cells (top) (y axis).

(E–G) (E) Visualization and (F and G) quantification of caspase-3 (magenta) expression. Scale bars, 50 μm. The representative images are from three independent experiments. Two-sided t test (n = 3 independent devices per group).

Data are presented as mean ± SEM. *$p < 0.05$; **$p < 0.01$.

signal in the endothelial channel (Figures 4F and 4G). Cumulatively, these data indicate that this EVT-driven EC remodeling was limited when the IOC device was exposed to type I IFN.

DISCUSSION

Elevated type I IFN during embryo implantation is associated with abnormal placentation and adverse pregnancy outcomes, suggesting a role for type I IFN in affecting EVT function. We designed this study to evaluate the consequence of unwarranted systemic IFN on EVT function using a biomimetic model of human implantation in an organ-on-a-chip device.[11] We found that elevated type I IFN in the IOC device limited EVT invasion and invading EVT emergence. In evaluation of IFN-exposed EVTs, we uncovered that sustained IFN signaling stunted EVT epithelial-to-mesenchymal progression with mesenchymal genes considerably reduced in all IFN-stimulated EVTs. Prior literature has indicated that IFN signaling is important for proper endometrial decidualization and spiral artery remodeling, yet the functional contribution of IFN signaling during implantation remained undefined.[3,4] Intriguingly, taken together with our findings, we speculate that there could be an IFN signaling paradigm that fine-tunes EMT transition in EVTs and thereby putatively facilitates depth of invasion and may be pathogenic under

situations of high, unwarranted type I IFN, such as in SLE. Nevertheless, further studies are needed to directly address this model.

Additionally, our work intended to investigate the impact of unwarranted IFN on implantation in order to mimic systemically elevated IFN in the environmental milieu, as seen in patients with SLE. As such, one limitation to our study is that we only transcriptionally assessed one time point with a single, high dose of IFN, thereby limiting our ability to distinguish nuances of dose. Further, previous studies have found that addition of other cell types found at the maternal-fetal interface in the IOC device, such as stromal cells or decidual immune cells, can influence EVT invasion.[5,11] The microfluidics of our IOC device does not allow us to individually treat ECs or EVTs, thus we cannot conclude direct or indirect effects of type I IFN on altered EVT function. Further, our current experimental setup does not include additional cell types; thus, an important future direction is to consider the added complexity of other IFN-responsive stromal and/or immune cells with known functions in facilitating EVT invasion and maternal spiral artery remodeling, such as uterine natural killer cells.[4,11]

Although our findings describe a change in EVT trajectory and state after elevated IFN exposure, our results do not rule out a role for endothelial-specific IFN response on EVT invasion. Previous work with the IOC device indicated a critical role for intercellular communication between maternal endometrial EC in mediating directional EVT migration and invasion, likely through secretion of an unknown factor(s).[11] Our studies did not address if IFN in ECs might impact this critical intercellular communication. Furthermore, our study only assessed an *in vivo* setting where there is IFN exposure on both maternal and fetal cells; therefore, future work is needed to decipher individual contributions of cell types to the altered EVT function triggered by IFN signaling.

We identified a PE-like signature in IFN-EVTs compared with controls. PE is a life-threatening hypertensive disorder of pregnancy that confers a long-term, increased risk of cardiovascular disease in both mother and child.[41] PE is a multifactorial disease with multicomponent risk; thereby, in order to effectively combat the disease, there is a need to distinguish underlying mechanisms of the various risk factors. Currently, PE is understood to occur in two stages with insufficient implantation and vascular remodeling leading to reduced placental perfusion (stage 1) that can lead to clinical manifestations of disease (stage 2).[42] Interestingly, we found induction of genes that are implicated in both stages of PE. We found that IFN stimulation induced the expression of known PE risk factors, such as complement activation. Aberrant activation of the complement system during first trimester is associated with the onset of PE later in gestation and thereby considered a stage 1 risk factor.[33,34] Furthermore, we identified noteworthy overlap with PE dysregulated genes that are known to be increased in stage 2 of PE, such as SAT1. SAT1 has been bioinformatically associated with PE physiopathology multiple times throughout literature, although the underlying mechanism remains poorly explored.[43,44] Overall, our study strikingly implicates unwarranted IFN signaling as a maternal disturbance that could trigger PE.

Overall, our work implicates elevated systemic type I IFN as a maternal disturbance that can result in abnormal EVT function that could instigate PE.

Limitations of the study

This work suggests that elevated systemic type I IFN alters invasive EVT function. A limitation of our study is the inability to distinguish direct or indirect effects of type I IFN on EVT function since the microfluidics of our IOC device does not allow us to individually treat ECs or EVTs. Another limitation of our experimental design is that it does not model the cellular complexity at implantation sites, such as the presence of stromal and/or immune cells. Future experiments could evaluate EVT- and EC-specific IFN responses and/or their interplay with other IFN-responsive cell types present at the maternal-fetal interface to provide additional mechanistic insights.

RESOURCE AVAILABILITY

Lead contact

Requests for further information and resources should be directed to and will be fulfilled by the lead contact, Kellie A. Jurado (kellie.jurado@pennmedicine.upenn.edu).

Materials availability

This study did not generate new unique reagents.

Data and code availability

- Single-cell RNA-seq data have been deposited at National Center for Biotechnology Information: NCBI BioProject: PRJNA1118265 and are publicly available as of the date of publication.
- Microscopy data reported in this paper will be shared by the lead contact upon request.
- All original code has been deposited at Zenodo at 10.5281/zenodo.11389981 and is publicly available as of the date of publication.
- Any additional information required to reanalyze the data reported in this paper is available from the lead contact upon request.

ACKNOWLEDGMENTS

We thank the members of the Jurado laboratory for helpful discussions on this study. We acknowledge support of the Center for Applied Genomics core facility at the Children's Hospital of Philadelphia.

We gratefully acknowledge support from the Chan Zuckerberg Initiative (Single-Cell Analysis of Inflammation; K.A.J., M.M., and D.D.H.) in addition to the following agencies/foundations: Clinical and Translational Science Award TL1TR001880 to M.K.S., University of Pennsylvania Presidential Fellowship to S.G.N., HHMI Gilliam Fellowship to M.C.A., and The Pew Charitable Trust (Biomedical Fellow) and Burroughs Wellcome Fund (Next Gen Pregnancy) to K.A.J.

AUTHOR CONTRIBUTIONS

M.K.S.: methodology, investigation, data curation, formal analysis, and writing – original draft. S.G.N.: data curation, formal analysis, visualization, and writing – review and editing. J.Y.P.: investigation, data curation, and formal analysis. S.M.: methodology, investigation, and writing – review and editing. M.C.A.: investigation and writing – review and editing. K.R.A.: formal analysis. D.D.H.: methodology, resources, supervision, and writing – review and editing. M.M.: conceptualization, methodology, funding acquisition, resources, supervision, and writing – review and editing. K.A.J.: conceptualization, methodology, data curation, formal analysis, funding acquisition, resources, supervision, and writing – original draft.

DECLARATION OF INTERESTS

The authors declare no competing interests.

STAR★METHODS

Detailed methods are provided in the online version of this paper and include the following:

- KEY RESOURCES TABLE
- EXPERIMENTAL MODEL AND STUDY PARTICIPANT DETAILS
  - Obtaining human samples
  - Primary cell isolation and culture
- METHOD DETAILS
  - Implantation-on-chip model
  - IOC treatments and immunofluorescence
- QUANTIFICATION AND STATISTICAL ANALYSIS
  - Quantification of EVT invasion
  - Single cell RNA sequencing

SUPPLEMENTAL INFORMATION

Supplemental information can be found online at https://doi.org/10.1016/j.xcrm.2025.101991.

Received: May 16, 2024
Revised: December 6, 2024
Accepted: February 5, 2025
Published: March 6, 2025

REFERENCES

1. Yockey, L.J., and Iwasaki, A. (2018). Interferons and proinflammatory cytokines in pregnancy and fetal development. Immunity *49*, 397–412. https://doi.org/10.1016/j.immuni.2018.07.017.
2. Pollheimer, J., Vondra, S., Baltayeva, J., Beristain, A.G., and Knöfler, M. (2018). Regulation of Placental Extravillous Trophoblasts by the Maternal Uterine Environment. Front. Immunol. *9*, 2597. https://doi.org/10.3389/fimmu.2018.02597.
3. Yamamoto, Y., Kurohmaru, M., and Hayashi, Y. (1992). Localization of type I interferon in murine trophoblast and decidua during decidual formation. J. Reprod. Fertil. *95*, 559–565. https://doi.org/10.1530/jrf.0.0950559.
4. Casazza, R.L., Lazear, H.M., and Miner, J.J. (2020). Protective and Pathogenic Effects of Interferon Signaling During Pregnancy. Viral Immunol. *33*, 3–11. https://doi.org/10.1089/vim.2019.0076.
5. Mani, S., Garifallou, J., Kim, S.-J., Simoni, M.K., Huh, D.D., Gordon, S.M., and Mainigi, M. (2024). Uterine macrophages and NK cells exhibit population and gene-level changes after implantation but maintain pro-invasive properties. Front. Immunol. *15*, 1364036. https://doi.org/10.3389/fimmu.2024.1364036.
6. Clowse, M.E.B., Magder, L.S., Witter, F., and Petri, M. (2006). Early risk factors for pregnancy loss in lupus. Obstet. Gynecol. *107*, 293–299. https://doi.org/10.1097/01.AOG.0000194205.95870.86.
7. Hong, S., Banchereau, R., Maslow, B.-S.L., Guerra, M.M., Cardenas, J., Baisch, J., Branch, D.W., Porter, T.F., Sawitzke, A., Laskin, C.A., et al. (2019). Longitudinal profiling of human blood transcriptome in healthy and lupus pregnancy. J. Exp. Med. *216*, 1154–1169. https://doi.org/10.1084/jem.20190185.
8. Clowse, M.E.B. (2007). Lupus Activity in Pregnancy. Rheum. Dis. Clin. North Am. *33*, 237–v. https://doi.org/10.1016/j.rdc.2007.01.002.
9. Andrade, D., Kim, M., Blanco, L.P., Karumanchi, S.A., Koo, G.C., Redecha, P., Kirou, K., Alvarez, A.M., Mulla, M.J., Crow, M.K., et al. (2015). Interferon-α and angiogenic dysregulation in pregnant lupus patients who develop preeclampsia. Arthritis Rheumatol. *67*, 977–987. https://doi.org/10.1002/art.39029.
10. Chakravarty, E.F., Nelson, L., and Krishnan, E. (2006). Obstetric hospitalizations in the United States for women with systemic lupus erythematosus and rheumatoid arthritis. Arthritis Rheum. *54*, 899–907. https://doi.org/10.1002/art.21663.
11. Park, J.Y., Mani, S., Clair, G., Olson, H.M., Paurus, V.L., Ansong, C.K., Blundell, C., Young, R., Kanter, J., Gordon, S., et al. (2022). A microphysiological model of human trophoblast invasion during implantation. Nat. Commun. *13*, 1252. https://doi.org/10.1038/s41467-022-28663-4.
12. Buchrieser, J., Degrelle, S.A., Couderc, T., Nevers, Q., Disson, O., Manet, C., Donahue, D.A., Porrot, F., Hillion, K.-H., Perthame, E., et al. (2019). IFITM proteins inhibit placental syncytiotrophoblast formation and promote fetal demise. Science *365*, 176–180. https://doi.org/10.1126/science.aaw7733.
13. Arutyunyan, A., Roberts, K., Troulé, K., Wong, F.C.K., Sheridan, M.A., Kats, I., Garcia-Alonso, L., Velten, B., Hoo, R., Ruiz-Morales, E.R., et al. (2023). Spatial multiomics map of trophoblast development in early pregnancy. Nature *616*, 143–151. https://doi.org/10.1038/s41586-023-05869-0.
14. Zhou, Y., Fisher, S.J., Janatpour, M., Genbacev, O., Dejana, E., Wheelock, M., and Damsky, C.H. (1997). Human cytotrophoblasts adopt a vascular phenotype as they differentiate. A strategy for successful endovascular invasion? J. Clin. Investig. *99*, 2139–2151. https://doi.org/10.1172/JCI119387.
15. Govindasamy, N., Long, H., Jeong, H.-W., Raman, R., Özcifci, B., Probst, S., Arnold, S.J., Riehemann, K., Ranga, A., Adams, R.H., et al. (2021). 3D biomimetic platform reveals the first interactions of the embryo and the maternal blood vessels. Dev. Cell *56*, 3276–3287.e8. https://doi.org/10.1016/j.devcel.2021.10.014.
16. Aplin, J.D., Jones, C.J.P., and Harris, L.K. (2009). Adhesion molecules in human trophoblast - a review. I. Villous trophoblast. Placenta *30*, 293–298. https://doi.org/10.1016/j.placenta.2008.12.001.
17. Street, K., Risso, D., Fletcher, R.B., Das, D., Ngai, J., Yosef, N., Purdom, E., and Dudoit, S. (2018). Slingshot: cell lineage and pseudotime inference for single-cell transcriptomics. BMC Genom. *19*, 477. https://doi.org/10.1186/s12864-018-4772-0.
18. Trapnell, C., Cacchiarelli, D., Grimsby, J., Pokharel, P., Li, S., Morse, M., Lennon, N.J., Livak, K.J., Mikkelsen, T.S., and Rinn, J.L. (2014). The dynamics and regulators of cell fate decisions are revealed by pseudotemporal ordering of single cells. Nat. Biotechnol. *32*, 381–386. https://doi.org/10.1038/nbt.2859.
19. La Manno, G., Soldatov, R., Zeisel, A., Braun, E., Hochgerner, H., Petukhov, V., Lidschreiber, K., Kastriti, M.E., Lönnerberg, P., Furlan, A., et al. (2018). RNA velocity of single cells. Nature *560*, 494–498. https://doi.org/10.1038/s41586-018-0414-6.
20. DaSilva-Arnold, S.C., Zamudio, S., Al-Khan, A., Alvarez-Perez, J., Mannion, C., Koenig, C., Luke, D., Perez, A.M., Petroff, M., Alvarez, M., and Illsley, N.P. (2018). Human trophoblast epithelial-mesenchymal transition in abnormally invasive placenta. Biol. Reprod. *99*, 409–421. https://doi.org/10.1093/biolre/ioy042.
21. DaSilva-Arnold, S., James, J.L., Al-Khan, A., Zamudio, S., and Illsley, N.P. (2015). Differentiation of first trimester cytotrophoblast to extravillous trophoblast involves an epithelial-mesenchymal transition. Placenta *36*, 1412–1418. https://doi.org/10.1016/j.placenta.2015.10.013.
22. E Davies, J., Pollheimer, J., Yong, H.E.J., Kokkinos, M.I., Kalionis, B., Knöfler, M., and Murthi, P. (2016). Epithelial-mesenchymal transition during extravillous trophoblast differentiation. Cell Adh. Migr. *10*, 310–321. https://doi.org/10.1080/19336918.2016.1170258.
23. Natenzon, A., McFadden, P., DaSilva-Arnold, S.C., Zamudio, S., and Illsley, N.P. (2022). Diminished trophoblast differentiation in early onset preeclampsia. Placenta *120*, 25–31. https://doi.org/10.1016/j.placenta.2022.02.004.
24. Ma, Z., Lou, S., and Jiang, Z. (2020). PHLDA2 regulates EMT and autophagy in colorectal cancer via the PI3K/AKT signaling pathway. Aging (Albany NY) *12*, 7985–8000. https://doi.org/10.18632/aging.103117.

25. Li, Z., Liu, J., Chen, T., Sun, R., Liu, Z., Qiu, B., Xu, Y., and Zhang, Z. (2021). HMGA1-TRIP13 axis promotes stemness and epithelial mesenchymal transition of perihilar cholangiocarcinoma in a positive feedback loop dependent on c-Myc. J. Exp. Clin. Cancer Res. *40*, 86. https://doi.org/10.1186/s13046-021-01890-1.

26. Luo, Y., Li, W., and Liao, H. (2013). HMGA2 induces epithelial-to-mesenchymal transition in human hepatocellular carcinoma cells. Oncol. Lett. *5*, 1353–1356. https://doi.org/10.3892/ol.2013.1193.

27. WEI Lirong, T.X. (2020). STC1 induces epithelial-mesenchymal transition to promote invasion and migration of lung cancer cells. China Oncology *30*, 497–504. https://doi.org/10.19401/j.cnki.1007-3639.2020.07.003.

28. Zhang, J., Chen, W.-Q., Yang, K., Wang, Z.-X., Sun, D.-L., Peng, Y.-Y., Yu, M., Wang, S.-X., and Guo, Q. (2023). RBM25 induces trophoblast epithelial-mesenchymal transition and preeclampsia disorder by enhancing the positive feedback loop between Grhl2 and RBM25. Exp. Biol. Med. *248*, 1267–1277. https://doi.org/10.1177/15353702231191199.

29. Illsley, N.P., DaSilva-Arnold, S.C., Zamudio, S., Alvarez, M., and Al-Khan, A. (2020). Trophoblast invasion: Lessons from abnormally invasive placenta (placenta accreta). Placenta *102*, 61–66. https://doi.org/10.1016/j.placenta.2020.01.004.

30. Fenstad, M.H., Johnson, M.P., Roten, L.T., Aas, P.A., Forsmo, S., Klepper, K., East, C.E., Abraham, L.J., Blangero, J., Brennecke, S.P., et al. (2010). Genetic and molecular functional characterization of variants within TNFSF13B, a positional candidate preeclampsia susceptibility gene on 13q. PLoS One *5*, e12993. https://doi.org/10.1371/journal.pone.0012993.

31. Xiong, Y., Zhou, Q., Jiang, F., Zhou, S., Lou, Y., Guo, Q., Liang, W., Kong, D., Ma, D., and Li, X. (2010). Changes of plasma and placental tissue factor pathway inhibitor-2 in women with preeclampsia and normal pregnancy. Thromb. Res. *125*, e317–e322. https://doi.org/10.1016/j.thromres.2010.02.017.

32. Palei, A.C., Cruz, J.d.O., Chaguri, J.L., Peraçoli, J.C., Romão-Veiga, M., Ribeiro-Vasques, V.R., Cavalli, R.C., Nunes, P.R., Luizon, M.R., and Sandrim, V.C. (2023). Circulating levels of tissue inhibitor of metalloproteinase 3, a protein with inhibitory effects on angiogenesis, are increased in preeclampsia. Int. J. Gynaecol. Obstet. *161*, 544–551. https://doi.org/10.1002/ijgo.14552.

33. He, Y.-D., Xu, B.-N., Wang, M.-L., Wang, Y.-Q., Yu, F., Chen, Q., and Zhao, M.-H. (2020). Dysregulation of complement system during pregnancy in patients with preeclampsia: A prospective study. Mol. Immunol. *122*, 69–79. https://doi.org/10.1016/j.molimm.2020.03.021.

34. Lokki, A.I., Ren, Z., Triebwasser, M., Daly, E., Daly, M., , et al.FINNPEC, Perola, M., Perola, M., Auro, K., Burwick, R., Salmon, J.E. (2023). Identification of complement factor H variants that predispose to pre-eclampsia: A genetic and functional study. A genetic and functional study. BJOG. *130*, 1473–1482. https://doi.org/10.1111/1471-0528.17529.

35. Admati, I., Skarbianskis, N., Hochgerner, H., Ophir, O., Weiner, Z., Yagel, S., Solt, I., and Zeisel, A. (2023). Two distinct molecular faces of preeclampsia revealed by single-cell transcriptomics. Med *4*, 687–709.e7. https://doi.org/10.1016/j.medj.2023.07.005.

36. Wang, J., Feng, Q., Liang, D., and Shi, J. (2021). MiRNA-26a inhibits myocardial infarction-induced apoptosis by targeting PTEN via JAK/STAT pathways. Cells Dev. *165*, 203661. https://doi.org/10.1016/j.cdev.2021.203661.

37. Zhang, P., Lu, H., Wu, Y., Lu, D., Li, C., Yang, X., Chen, Z., Qian, J., and Ge, J. (2023). COX5A Alleviates Doxorubicin-Induced Cardiotoxicity by Suppressing Oxidative Stress, Mitochondrial Dysfunction and Cardiomyocyte Apoptosis. Int. J. Mol. Sci. *24*, 10400. https://doi.org/10.3390/ijms241210400.

38. Wu, C., Yan, L., Depre, C., Dhar, S.K., Shen, Y.-T., Sadoshima, J., Vatner, S.F., and Vatner, D.E. (2009). Cytochrome c oxidase III as a mechanism for apoptosis in heart failure following myocardial infarction. Am. J. Physiol. Cell Physiol. *297*, C928–C934. https://doi.org/10.1152/ajpcell.00045.2009.

39. Luan, Y., Tang, N., Yang, J., Liu, S., Cheng, C., Wang, Y., Chen, C., Guo, Y.-N., Wang, H., Zhao, W., et al. (2022). Deficiency of ribosomal proteins reshapes the transcriptional and translational landscape in human cells. Nucleic Acids Res. *50*, 6601–6617. https://doi.org/10.1093/nar/gkac053.

40. Márquez-Jurado, S., Díaz-Colunga, J., das Neves, R.P., Martinez-Lorente, A., Almazán, F., Guantes, R., and Iborra, F.J. (2018). Mitochondrial levels determine variability in cell death by modulating apoptotic gene expression. Nat. Commun. *9*, 389. https://doi.org/10.1038/s41467-017-02787-4.

41. Bokslag, A., van Weissenbruch, M., Mol, B.W., and de Groot, C.J.M. (2016). Preeclampsia; short and long-term consequences for mother and neonate. Early Hum. Dev. *102*, 47–50. https://doi.org/10.1016/j.earlhumdev.2016.09.007.

42. Roberts, J.M., and Hubel, C.A. (2009). The Two Stage Model of Preeclampsia: Variations on the Theme. Placenta *30*, S32–S37. https://doi.org/10.1016/j.placenta.2008.11.009.

43. Tejera, E., Bernardes, J., and Rebelo, I. (2012). Preeclampsia: a bioinformatics approach through protein-protein interaction networks analysis. BMC Syst. Biol. *6*, 97. https://doi.org/10.1186/1752-0509-6-97.

44. Shi, M., Yang, X., Ding, Y., Sun, L., Zhang, P., Liu, M., Han, X., Huang, Z., and Li, R. (2022). Ferroptosis-Related Proteins Are Potential Diagnostic Molecular Markers for Patients with Preeclampsia. Biology *11*, 950. https://doi.org/10.3390/biology11070950.

45. Graham, C.H., Lysiak, J.J., McCrae, K.R., and Lala, P.K. (1992). Localization of transforming growth factor-beta at the human fetal-maternal interface: role in trophoblast growth and differentiation. Biol. Reprod. *46*, 561–572. https://doi.org/10.1095/biolreprod46.4.561.

46. Griffiths, J.A., Richard, A.C., Bach, K., Lun, A.T.L., and Marioni, J.C. (2018). Detection and removal of barcode swapping in single-cell RNA-seq data. Nat. Commun. *9*, 2667. https://doi.org/10.1038/s41467-018-05083-x.

47. Lun, A.T.L., Riesenfeld, S., Andrews, T., Dao, T.P., Gomes, T., and Marioni, J.C.; participants in the 1st Human Cell Atlas Jamboree (2019). EmptyDrops: distinguishing cells from empty droplets in droplet-based single-cell RNA sequencing data. Genome Biol. *20*, 63. https://doi.org/10.1186/s13059-019-1662-y.

48. McGinnis, C.S., Murrow, L.M., and Gartner, Z.J. (2019). DoubletFinder: Doublet Detection in Single-Cell RNA Sequencing Data Using Artificial Nearest Neighbors. Cell Syst. *8*, 329–337.e4. https://doi.org/10.1016/j.cels.2019.03.003.

STAR★METHODS

KEY RESOURCES TABLE

REAGENT or RESOURCE	SOURCE	IDENTIFIER
Antibodies		
Caspase-3 (1:200)	Cell Signaling Technology	Cat#9661; RRID: AB_2341188
PECAM1 (1:200)	BioLegend	Cat#910003; RRID: AB_2565394
Ki67 (1:200)	Abcam	Cat#ab245113; RRID: AB_2923193
HLA-G (1:100)	Biorad	Cat#MCA2044; RRID: AB323364
Cytokeratin-7 (1:100)	Abcam	Cat#ab181598; RRID: AB_2783822
Biological samples		
Primary Human Extravillous Trophoblasts	This manuscript	N/A
Primary Human Endometrial Endothelial cells (HEMEC)	ScienCell	Cat#7010
Chemicals, peptides, and recombinant proteins		
Recombinant Human IFN-β	PeproTech	Cat#300-02BC
Critical commercial assays		
CellTracker Green CMFDA	Thermo Fisher Scientific	Cat# C7025
10x Genomics Chromium Single Cell 3′ Reagent kit	10x Genomics	V 3
Deposited data		
Raw data	This manuscript	NCBI BioProject: PRJNA1118265
Original code	This manuscript	Zenodo: 10.5281/zenodo.11389981
Software and algorithms		
Cell Ranger	10x Genomics	V 6.0.0
Cell Ranger	10x Genomics	V 7.3.0
R Studio	https://posit.co/products/open-source/rstudio/	"Prairie Trillium" Release
ImageJ	https://imagej.nih.gov/ij/notes.html	Version 1.53
Graphpad Prism	https://www.graphpad.com/scientific-software/prism/	Version 10.0.1
Biorender	https://biorender.com/	N/A

EXPERIMENTAL MODEL AND STUDY PARTICIPANT DETAILS

Primary human extravillous trophoblasts and endothelial cells were used for the implantation-on-chip model. Further details are provided in the method details section.

Obtaining human samples

Placental villi were obtained per protocol from first-trimester pregnancy terminations performed at the Penn Family and Pregnancy Loss Center (IRB#827072) (n = 3, gestational ages 6–11 weeks). All subjects were counseled appropriately and provided written informed consent. Patients with preexisting medical conditions known to be associated with poor reproductive outcomes or any pregnancy complications in the current pregnancy were excluded from the study. Collected tissue was kept on ice and cell isolation was carried out within 1 h of procurement.

Primary cell isolation and culture

Primary Human Extravillous Trophoblasts: Primary EVTs were isolated from first trimester termination tissue based on an EVT-outgrowth based protocol established by Graham et al.[45] Briefly, villous tissue was finely minced and cultured at 37°C in RPMI 1640 medium containing 20% charcoal-stripped fetal bovine serum (FBS, Gibco, Catalog # 10437). After villous fragment attachment, EVT outgrowth occurred, and cells were separated from tissue during washing and passaging of the cells. The isolated

EVTs were then cultured in 6 well plates using RPMI 1640 medium containing 20% FBS and 1% penicillin (100 U/ml)/streptomycin (100 U/ml). The cultured EVTs were used for constructing the implantation-on-a-chip model within the first 3 passages. EVT identity of the cells used in our experiments were characterized by immunostaining of cytokeratin-7 and HLA-G.

Primary Human Endometrial Endothelial cells: Human endometrial microvascular endothelial cells were purchased (HEMEC, ScienCell, catalog #7010) and cultured in Endothelial Cell Growth Medium MV2 (EGM-MV2, Promocell, catalog # C-22022).

METHOD DETAILS

Implantation-on-chip model

The 3-chamber device used to physiologically and spatially model EVT invasion is originally described and validated in a prior publication.[37] In brief, the fully enclosed device contains three parallel chambers, each individually accessible to fill with media and/or cells of choice. In our model, the middle chamber contains an extracellular matrix (ECM) to represent the endometrial stroma Primary human EVTs are in one side chamber (the "fetal" chamber), and human endometrial endothelial cells in the other (the "vascular" chamber), across the ECM. The arrangement allows in vivo-like directional migration of EVTs toward a micro-engineered maternal vessel to represent a physiologically relevant human model system (Figures 1A–1D).

The ECM is a hydrogel precursor solution composed of a rat tail collagen Type-1 and Matrigel. Maternal endothelial cells and extravillous trophoblasts were cultured in their respective chambers, with media replenished every day. PromoCell Endothelial Cell Growth Medium MV2 (ready to use) media (C-22022) was used for the vascular chamber, and RPMI +2% FBS was used for the fetal chamber. The flow of media was prevented to simulate occluded blood flow at the maternal-fetal interface, with extra precautions taken during media exchange to minimize disruption of the culture environment. EVTs were fluorescently labeled with 5 μg/mL of CellTracker Green CMFDA (Thermo Fisher Scientific, Waltham, MA, USA, catalog #C7025) per manufacturer protocol in DMEM supplemented 2% (v/v) FBS for 15 min at 37°C, respectively. The device was incubated in a cell culture incubator in normoxic conditions maintained at 5% CO2.

IOC treatments and immunofluorescence

After an initial 48 h, the fetal and vascular chambers were treated with 100 or 1000 IU/mL of IFN-β with respective media and replaced every 24 h (Figure 1C). Devices were imaged at 24, 72 and 120 h after initial addition of IFN-β. After completion of cell culture experiments, media were removed from the reservoirs, and the channels were washed 3 times by flowing PBS. Cells cultured in flasks were similarly treated. Cells were fixed by introducing 4% paraformaldehyde (PFA, Thermo Scientific, catalog # AAJ19943K2) into the channels and incubated for 30 min at room temperature (RT), followed by 3 washes with PBS for all immunofluorescence experiments. After cell permeabilization and blocking with 0.1% Triton X- and 1% bovine serum albumin (BSA, Sigma, catalog # 5217), respectively, the cells were incubated with primary antibodies against Caspase-3 (Asp175, Cell Signaling, catalog # 9661), PECAM1 (2HB, Developmental Studies Hybridoma Bank) and Ki67 (37C7-12, Abcam, catalog # ab245113) diluted at 1:200 in 1% BSA-containing PBS solution at 4°C overnight. For EVT cultures, HLA-G (MEM-G/9, Biorad, catalog # MCA2044) and Cytokeratin-7 (EPR17078, Abcam, catalog # ab181598) antibody was used at 1:100 dilution. Subsequently, the cells were washed 3 times by flowing PBS and treated with appropriate secondary antibodies diluted at 1:200 in PBS containing 1% BSA for 2 h at room temperature. The cells were counterstained with DAPI, then washed with PBS three times. Fluorescence imaging was performed using an inverted microscope with confocal capabilities (LSM 800, Carl Zeiss, Germany; 10×0.45 NA objectives).

QUANTIFICATION AND STATISTICAL ANALYSIS

Quantification of EVT invasion

Fluorescence images of EVTs were obtained from the ECM matrix region between the maternal vascular and fetal compartments of the implantation-on-a-chip device. High magnification images were collected from three separate devices per each experimental group with three representative images per device. EVT invasion was quantified at 24, 72 and 120 h after addition of IFN-β, by (i) the number of invading EVTs and (ii) the area of EVT invasion. To evaluate the cell number, EVTs in the ECM compartments were manually counted, and the average of total cell counts was plotted. The invasion depth was also calculated at 120 h and quantified by the sum of the vertical travel distances of all EVTs in a given field of view divided by the total number of EVTs in the same imaging area to calculate the average depth of invasion per cell number. Each data point in the invasion depth plots represents the mean of the average invasion depths measured from three randomly selected areas within a single device. Analysis of invasion area was achieved by using the Analyze pixels function of ImageJ (NIH) with appropriate thresholding to measure the area of ECM hydrogel covered by invading EVTs. A one-way ANOVA was performed to compare means, and a p-value <0.05 was considered statistically significant using GraphPad Prism. Additional statistical details of experiments can be found in figure legends.

Single cell RNA sequencing

Six IOC experiments per patient per condition (Control vs. IFN-β) were run to analyze scRNA-sequencing, for a total of 36 devices. The IFN-β experiments used a dose of 1000 IU/mL of IFN-β based on the results seen in the invasion studies and increased the likelihood of establishing a difference between experimental groups. To assess the cells in the devices at the end of experiments, media

was removed, and the devices were washed twice with PBS. After removing residual PBS, the reservoirs of each channel were filled with 0.25% Trypsin and incubated at 37°C for 15 min while pipetting every 5 min until the ECM hydrogel in the middle channel was completely dissolved. Cell suspensions were collected, centrifuged at 300 × g for 5 min, and then the supernatant was removed using a pipette, leaving only the cell pellet. Cells were then washed in MACS buffer (sterile PBS, 1% FBS, 2 mM EDTA).

Next-generation sequencing libraries were prepared using the 10x Genomics Chromium Single Cell 3′ Reagent kit v3 as per manufacturer's instructions. Libraries were uniquely indexed using the Chromium i7 Sample Index Kit, pooled, and sequenced on the Illumina NovaSeq6000 sequencer in a paired-end, single indexing run. Sequencing for each library targeted 20,000 mean reads per cell. Data was then processed using the Cellranger pipeline (10x genomics, v.6.0.0) for demultiplexing and alignment of sequencing reads to the GRCh38 transcriptome and creation of feature-barcode matrices.

Raw data was processed with the *DropUtils* R package[46,47] to remove empty cells, and the *DoubletFinder* R package[48] to remove probable doublets. Downstream analysis was done using *Seurat* (v.4.0.4) in R. Cells included in the analysis had greater than 500, and less than 15000 transcripts, greater than 250 and less than 5000 detected genes, a "complexity" score (log10GenesPerUMI) greater than 0.8, and a mitochondrial gene expression ratio of less than 20%. Cells were normalized for cell cycle phase and mitochondrial content using the *sctransform* function. Cells were integrated using a canonical correlation analysis to expect similar biological states among at least a subset of single cells across the conditions. Clustering was achieved using the *FindClusters()* function in Seurat. This constructed a K-nearest-neighbors graph of cells, using between 1 and 20 canonical correlation vectors, and partitioned them into 'quasi-cliques' based on similar gene expression. A clustering resolution of 0.2 was used to optimize the biologic variability expected based on prior studies based on a *clustertree* analysis. Differentially expressed genes (DEGs) were determined via the *FindAllMarkers()* in Seurat. DEGs were considered significant if they were increased or decreased by at least 1 log2 fold change, utilizing a false detection rate of 5%. *Monocle3*, *slingshot* R,[17] and velocytoR[19] packages were used for pseudotime analysis of single-cell gene expression changes as a function of location and nearby cells.

For benchmarking purposes, we used sctransform and canonical correlation analysis in *Seurat* to further integrate scRNA-seq data of endovascular and interstitial EVTs from a study by Arutyunyan et al.[13] This reference data is of Donor P13, and publicly available via at https://www.reproductivecellatlas.org.